J|A|C|S
ARTICLES
Published on Web 01/20/2007

Solution-Phase Structural Characterization of Supramolecular Assemblies by Molecular Diffraction

Jodi L. O'Donnell,[†] Xiaobing Zuo,[§] Andrew J. Goshe,[§] Lev Sarkisov,[‡] Randall Q. Snurr,[‡] Joseph T. Hupp,[†] and David M. Tiede*[,§]

Contribution from the Department of Chemistry, Northwestern University, Evanston, Illinois 60208, Department of Chemical and Biological Engineering, Northwestern University, Evanston, Illinois 60208, and [†]Chemistry Division, Argonne National Laboratory, Argonne, Illinois 60439

Received August 14, 2006; Revised Manuscript Received November 28, 2006; E-mail: tiede@anl.gov

Abstract: Structures of four molecular squares based on rhenium coordination chemistry have been characterized in the solution phase using pair distribution function (PDF) analyses of wide-angle X-ray scattering measured to better than 1 Å spatial resolution. In this report we have focused, in particular, on a comparison of structures for pyrazine- and bipyridine-edged squares measured in solution with structures determined for these molecules in the solid state using X-ray crystallography and models derived from geometry optimization and molecular dynamics simulations using a classical force field. The wide-angle scattering for these assemblies is dominated by pair correlations involving one or more rhenium atoms, with both edge and diagonal Re−Re interactions appearing prominently in PDF plots. The pyrazine square is characterized by a relatively rigid structure in solution, with PDF peak positions and linewidths corresponding closely to those calculated from crystal structure data. For the bipyridine-edged square, the experimental PDF peaks measured along the molecular sides match the positions and linewidths of the PDF peaks calculated from static models. In contrast, PDF peaks measured across the diagonal distances of the molecular square deviate significantly from those calculated from the static crystallographic and energy minimized models. The experimental data are instead indicative of configurational broadening of the diagonal distances. In this respect, molecular dynamics simulations point to the importance of butterfly type motions that modulate the Re−Re diagonal distance. Indeed, the experimental data are reasonably well fit by assuming a bimodal distribution of butterfly conformers differing by ∼25° in the Re−Re−Re−Re torsion angle. Additionally, the measurements provide evidence for solvent ordering by the supramolecular assemblies detected as regions of solvent association and exclusion.

Introduction

The preparation of molecular squares, rectangles, triangles, and other polyhedra consisting of difunctional ligand edges coordinated to transition metal corners has been a major focus of coordination chemistry over the past decade.[1−4] Synthetic capabilities have advanced to the point that a ligand can be tailored to form a chosen polyhedron, ranging from dimeric to dodecameric, with assembly sizes ranging in diameter from 5 Å to over 35 Å. The synthetic efforts invested in building a substantial library of these supramolecules have enabled chemists to produce function-specific assemblies, including molecular filters,[5−7] nanoscale reaction vessels,[8,9] chemical sensors,[10−12] and catalysts or artificial enzymes.[13−16] While it is well-established that these polyhedra readily form, and spectroscopic evidence can often be cited as proof of formation of the desired assembly, exact structural characterization is often either difficult or impossible. Generally, large molecular polyhedra cannot be easily crystallized for X-ray crystal structure determination, although smaller assemblies (metal−metal distances of ca. 16

[†] Department of Chemistry, Northwestern University.
[‡] Department of Chemical and Biological Engineering, Northwestern University.
[§] Argonne National Laboratory.

(1) Fujita, M. *Chem. Soc. Rev.* **1998**, *27*, 417−425.
(2) Stang, P. J.; Olenyuk, B. *Acc. Chem. Res.* **1997**, *30*, 502−518.
(3) Dinolfo, P. H.; Hupp, J. T. *Chem. Mater.* **2001**, *13*, 3113−3125 and references therein.
(4) Holliday, B. J.; Mirkin, C. A. *Angew. Chem., Int. Ed.* **2001**, *40*, 2022−2043 and references therein.
(5) Williams, M. E.; Benkstein, K. D.; Abel, C.; Dinolfo, P. H.; Hupp, J. T. *Proc. Natl. Acad. Sci. U.S.A.* **2002**, *99*, 5171−5177.
(6) Keefe, M. H.; O'Donnell, J. L.; Bailey, R. C.; Nguyen, S. T.; Hupp, J. T. *Adv. Mater.* **2003**, *15*, 1936−1939.
(7) Czaplewski, K. F.; Hupp, J. T.; Snurr, R. Q. *Adv. Mater.* **2001**, *13*, 1895−1897.
(8) Yoshizawa, M.; Kusukawa, T.; Fujita, M.; Yamaguchi, K. *J. Am. Chem. Soc.* **2000**, *122*, 6311−6312.
(9) Yoshizawa, M.; Takeyama, Y.; Okano, T.; Fujita, M. *J. Am. Chem. Soc.* **2003**, *125*, 3243−3247.
(10) Sun, S.-S.; Lees, A. J. *J. Am. Chem. Soc.* **2000**, *122*, 8956−8967.
(11) Mines, G. A.; Tzeng, B.; Stevenson, K. J.; Li, J.; Hupp, J. T. *Angew. Chem., Int. Ed.* **2002**, *41*, 154−157.
(12) Keefe, M. H.; Slone, R. V.; Hupp, J. T.; Czaplewski, K. F.; Snurr, R. Q.; Stern, C. L. *Langmuir* **2000**, *16*, 3964−3970.
(13) Merlau, M. L.; Mejia, M. d. P.; Nguyen, S. T.; Hupp, J. T. *Angew. Chem., Int. Ed.* **2001**, *40*, 4239−4242.
(14) Fiedler, D.; Leung, D. H.; Bergman, R. G.; Raymond, K. N. *Acc. Chem. Res.* **2005**, *38*, 351−360.
(15) Sun, W. Y.; Kusukawa, T.; Fujita, M. *J. Am. Chem. Soc.* **2002**, *124*, 11570−11571.
(16) Lee, S. J.; Hu, A.; Lin, W. *J. Am. Chem. Soc.* **2002**, *124*, 12948−12949.

10.1021/ja0659065 CCC: $37.00 **© 2007 American Chemical Society**

Scheme 1

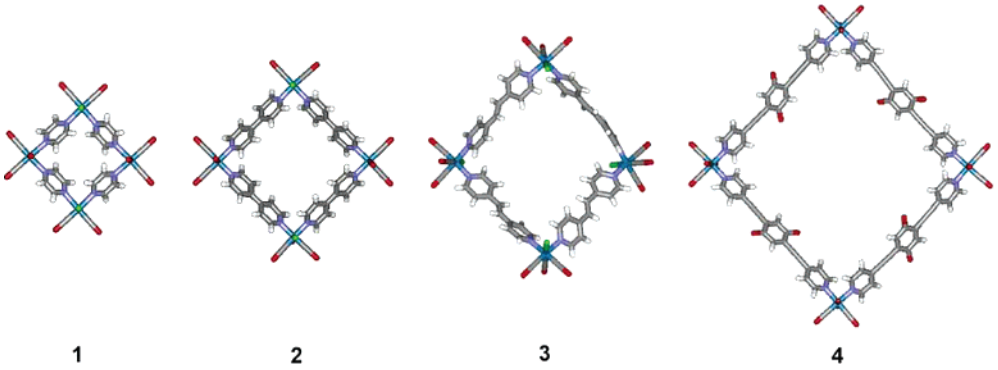

Å or less) often can be crystallized.[17,18] Furthermore, characterization of in situ conformational dynamics is critical for achieving a fundamental understanding of function at the atomic scale.

Traditional analyses such as NMR, IR, UV−vis, and elemental analysis are limited in their ability to distinguish between products such as cyclic trimers and tetramers.[10] Due to this limitation most researchers rely upon these techniques in conjunction with mass spectrometric data[19] or chromatographic analyses such as gel permeation chromatorgraphy[20] to ensure the pure formation of one assembly. Furthermore, many applications require structural information such as the catenation of rings, location of guests in host−guest assemblies, or cavity size based upon orientation of walls, which cannot easily be determined by traditional techniques. In addition, for most applications, the polyhedra are employed in either solution or thin-film form—environments where molecular structures could vary significantly from crystal structures.

Small-angle X-ray scattering has been extensively employed to gain information about the overall shape and size of noncrystalline proteins and macromolecules.[21−23] While the information obtained at small angles (typically $2\theta < 5°$) is valuable for structural characterization of the macromolecules in noncrystalline media, for example, allowing discrimination of cyclic versus open oligomers and detection of aggregation and stacking of molecules, high-resolution structural information is not available. By collecting scattering data at high angles, however, selected intramolecular distances can be directly resolved with a precision that approaches that of conventional X-ray powder or crystallographic measurements. Wide-angle X-ray scattering has been applied for characterization of the solution structures for a range of molecular and supramolecular species, including metal ion complexes,[24,25] DNA,[26,27] proteins,[28−32] and covalently linked macrocylic architectures.[33] The ability to measure intramolecular distances by wide-angle scattering is particularly significant for supramolecular chemistry, as it provides a direct and possibly unique means to determine geometry, including conformational and configurational dispersions that arise from macromolecular dynamics in solution.[26,27,33] Further, the development of coordinate-based analytical tools[27,33−35] makes possible a quantitative evaluation of models provided by X-ray diffraction, NMR, molecular modeling, or simulations.

Herein we report the characterization of four representative molecular squares, Scheme 1, based on rhenium coordination chemistry in solution phase with better than 1 Å resolution. We have focused, in particular, on pyrazine- and bipyridine-edged squares (**1** and **2**, respectively; Scheme 1) for which we have combined structural data from the solid-state using X-ray crystallography,[17,18] modeling using force field geometry optimization and molecular dynamics simulations, and the solution state using wide-angle scattering. The flexibility of previously measured covalent macrocycle architectures (hexaporphyrin structures) caused wide-angle interference patterns to be significantly damped due to relatively large amplitude intramolecular motions.[33] The molecular squares considered here are of interest because they are representative of a broad class of supramolecular architectures based on metal coordination chemistry that are expected to be more rigid than those based entirely on covalent connectivity. Further, the presence of electron dense metal atoms at corner positions with relatively simple hydrocarbon frameworks can be expected to provide well-defined reference points for precise intramolecular distance determination. Recently, Megyes and co-workers have used wide-angle scattering for the solution-phase structural characterization of cationic metallocyclic triangles and rectangles based on phenanthroline and anthracene cornerposts, respectively, and diplatinum bipyridyl spacers.[36] These experiments uncovered shifts in metal−metal distances that may reflect enhanced flexibility of the molecules in solution compared to the

(17) Bélanger, S.; Hupp, J. T.; Stern, C. L.; Slone, R. V.; Watson, D. F.; Carrell, T. G. *J. Am. Chem. Soc.* **1999**, *212*, 557−563.
(18) Slone, R. V.; Hupp, J. T.; Stern, C. L.; Schmitt, T. E. A. *Inorg. Chem.* **1996**, *35*, 4096−4097.
(19) Schalley, C. A.; Muller, T.; Linnartz, P.; Witt, M.; Schafer, M.; Lutzen, A. *Chem.—Eur. J.* **2002**, *8*, 3538−3551.
(20) Graves, C. R.; Merlau, M. L.; Morris, G. A.; Sun, S.-S.; Nguyen, S. T.; Hupp, J. T. *Inorg. Chem.* **2004**, *43*, 2013−2017.
(21) Svergun, D. I.; Feigin, L. A.; Taylor, G. W. *Structure Analysis by Small Angle X-ray and Neutron Scattering*; Plenum Press: New York, 1987.
(22) Glatter, O. In *Neutron, X-ray and Light Scattering*; Lindner, P., Zemb, T., Eds.; Elsevier Science Publishers B.V.: Amsterdam, 1991; pp 33−82.
(23) Guinier, A.; Fournet, G. *Small Angle Scattering*; Wiley: New York, 1955.
(24) Vaughan, P. A.; Sturdivant, J. H.; Pauling, L. *J. Am. Chem. Soc.* **1950**, *72*, 5477−5486.
(25) Megyes, T.; Schubert, G.; Kovács, M.; Radnai, T.; Gróss, T.; Bakó, I.; Pápai, I.; Horváth, A. *J. Phys. Chem. A* **2003**, *107*, 9903−9909.
(26) Zuo, X.; Tiede, D. M. *J. Am. Chem. Soc.* **2005**, *127*, 16−17.
(27) Zuo, X.; Cui, G.; Mertz, K. M.; Zhang, L.; Lewis, F. D.; Tiede, D. M. *Proc. Natl. Acad. Sci. U.S.A.* **2006**, *103*, 3534−3539.
(28) Fedorov, B. A.; Denesyuk, A. I. *J. Appl. Crystallogr.* **1978**, *11*, 473−477.
(29) Tiede, D. M.; Zhang, R.; Seifert, S. *Biochemistry* **2002**, *41*, 6605−6614.
(30) Hirai, M.; Iwase, H.; Hayakawa, T.; Miura, K.; Inoue, K. *J. Synchrotron Rad.* **2002**, *9*, 202−205.
(31) Fischetti, R. F.; Rodi, D. J.; Mirza, A.; Irving, T. C.; Kondrashkina, E.; Makowski, L. *J. Synchrotron Rad.* **2003**, *10*, 398−404.
(32) Fischetti, R. F.; Rodi, D. J.; Gore, D. B.; Makowski, L. *Chem. Biol.* **2004**, *11*, 1431−1443.
(33) Tiede, D. M.; Zhang, R.; Chen, L. X.; Yu, L.; Lindsey, J. S. *J. Am. Chem. Soc.* **2004**, *126*, 14054−14062.
(34) Svergun, D.; Barberato, C.; Koch, M. H. J. *J. Appl. Crystallogr.* **1995**, *28*, 768−773.

Scheme 2

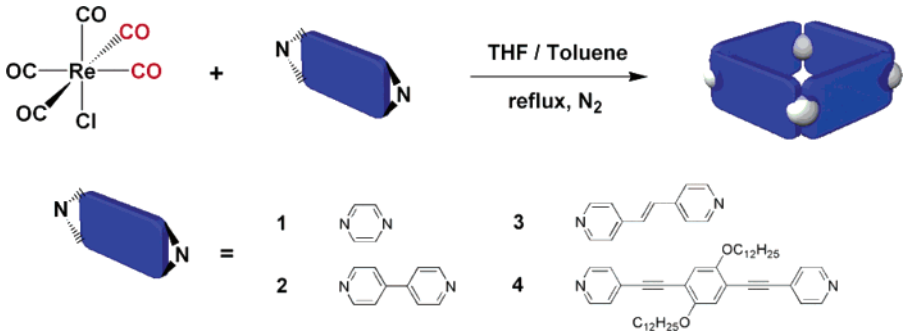

crystalline state[36] or changes in supramolecular conformation. In addition, measurements for these highly charged metallocycles showed prominent peaks due to solvent ordering.[36,37] While these "interferences" can hinder, or at least complicate, the determination of intramolecular atomic pair distances, they also represent a unique source of quantitative structural information about solvent/supramolecular−solute interactions.

In this report we have used wide-angle X-ray scattering for the characterization of the solution structure for a series of neutral molecular squares. To the first order, the absence of net charge removes complications due to solvent ordering,[25,36,37] and the simple rhenium cornerpost geometry makes possible the resolution of supramolecular conformation by measurement of Re−Re side and diagonal distances. We have compared experimental scattering patterns and corresponding real space pair distribution function (PDF) patterns for the solution state molecular squares to those calculated from crystallographic data and molecular simulations. This comparison has allowed us to index the goodness-of-fit between solution state experiments and coordinate models and to provide experimental benchmarks for more detailed atomistic modeling of solution state structure and configuration dispersion for rhenium polyhedra.

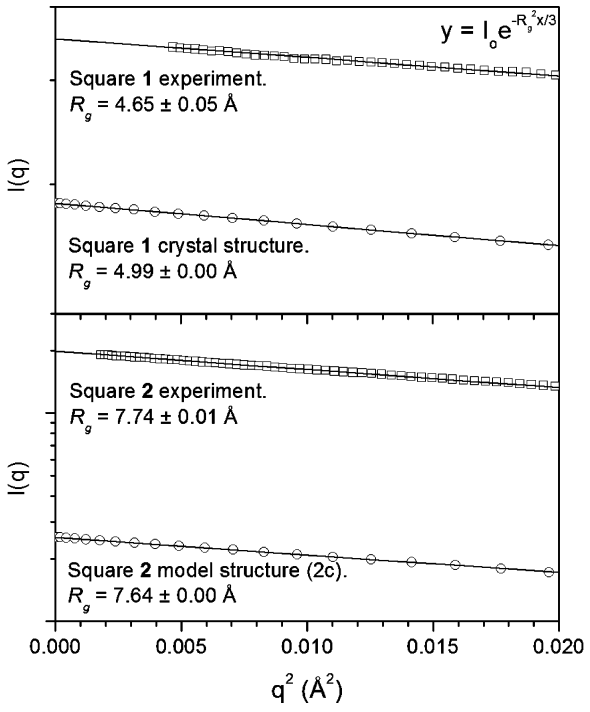

Figure 1. Guinier plots for calculated and experimental scattering data for **1** and **2.** The experimental data are arbitrarily offset in the vertical direction for clarity.

Results and Discussion

X-ray Scattering from Molecular Squares. Solution-phase scattering patterns were measured using samples in the millimolar concentration range. Since this is higher than typically considered for large supramolecular assemblies, it is necessary to ensure that the wide-angle scattering patterns are free of perturbations due to intermolecular association or aggregation. At very low q, X-ray scattering intensity as a function of the scattering vector q is described by the Guinier relationship, $I(q) = I(0)\exp(-q^2R_g^2/3)$, where $I(0)$ is proportional to the electron-density-contrast-weighted square of the number of electrons in the scattering object and R_g is the electron-density-weighted radius of gyration.[23] The scattering vector, q, is related to the scattering angle 2θ, by the equation $q = (4\pi/\lambda)\sin\theta$, where λ is the X-ray wavelength. Both $I(0)$ and R_g contain information on the overall size and aggregation state of the scattering particle.[23] Figure 1 compares Guinier plots of experimental scattering data for **1** and **2** compared to plots generated from coordinate models obtained from the crystal structure for **1** and a geometry optimized model for **2**. The choice of these reference model compounds is discussed below. The experimental R_g values for **1** and **2** as well as **3** and **4** agree well with sizes expected for monodisperse samples, Table 1.

Wide-angle X-ray scattering patterns for rhenium-based molecular squares show strong interference patterns dominated by beat frequencies corresponding to the rhenium spacing within the discrete squares. Although a large percentage of the total electron density within each square is located along the square walls in the bridging ligands, the concentration of electron density on the cornerposts due to heavy rhenium and halogen atoms is very high in comparison to the hydrocarbon ligands. The scattering patterns for several molecules with varying bridging ligand lengths are shown in Figure 2 recorded to a spatial resolution of 2.1 Å ($d = 2\pi/q$). The observed interference patterns are markers of overall macrocycle structure, molecular motions, configurational flexibility, and solvent interactions. Qualitatively, the molecular solution X-ray scattering patterns show an anticipated inverse relationship between real space Re−Re distances and reciprocal space Fourier frequencies and

(35) Zhang, R.; Thiyagarajan, P.; Tiede, D. M. *J. Appl. Crystallogr.* **2000**, *33*, 565−568.
(36) Megyes, T.; Jude, H.; Grósz, T.; Bakó, I.; Radnai, T.; Tárkányi, G.; Pálinkás, G.; Stang, P. J. *J. Am. Chem. Soc* **2005**, *127*, 10731−10738.
(37) Megyes, T.; Grósz, T.; Radnai, T.; Bakó, I.; Pálinkás, G. *J. Phys. Chem. A* **2004**, *108*, 7261−7271.

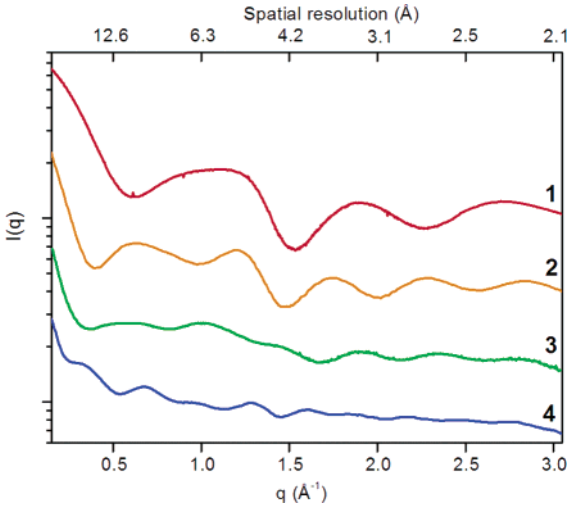

Figure 2. Intensity versus q plots for squares **1**−**4**. Larger interaction distance (d) yields smaller spacing (q) in reciprocal space, and Re−Re spacing dominates scattering. For clarity, patterns are arbitrarily vertically offset.

Table 1. Summary of Guinier Analysis of Molecular Square Assemblies

		R_g (Å)
1	model	4.99[a]
	experiment	4.65 ± 0.05
2	model	7.64[b]
	experiment	7.74 ± 0.01
3	model	9.27[b]
	experiment	10.52 ± 0.13
4	model	14.20[b]
	experiment	16.29 ± 0.09

[a] Obtained from single-crystal X-ray structure (ref 18). [b] Obtained from molecular mechanics modeling.

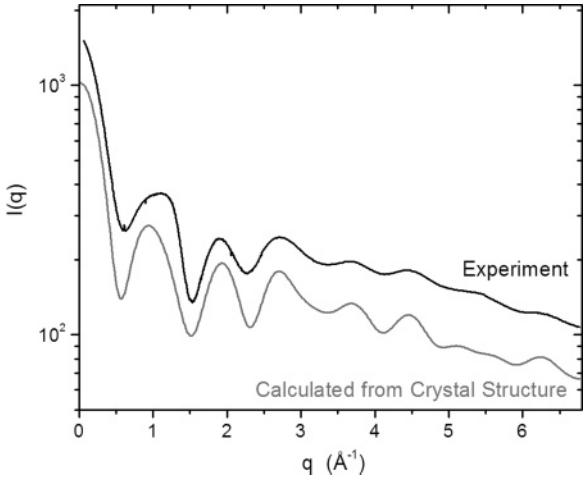

Figure 3. Experimental and calculated scattering patterns for **1**. The experimental scattering pattern was measured from a 1 mM solution in dimethylformamide. The calculated pattern was determined from the crystal structure of **1**.[18] The patterns are arbitrarily offset vertically.

Table 2. Summary of Molecular Assembly Size

		Re–Re side length (Å)
1	model	7.3[a]
	experiment	7.3
2	model	11.5[b]
	experiment	11.5
3	model	14.4[b]
	experiment	13.9
4	model	20.6[b]
	experiment	20.9

[a] Obtained from single-crystal X-ray structure (ref 18). [b] Obtained from molecular mechanics modeling.

positions of the first interference peak maximum. Re−Re edge distances determined from PDF analysis for **1**−**4** are tabulated in Table 2. These data agree well with those calculated from models and solid-state X-ray structures. The edge distance, however, is insensitive to supramolecular distortions, so agreement would be expected regardless of conformation. As described further below, a more detailed analysis of scattering patterns for **1** and **2**, chosen as representative compounds for the entire set of supramolecular species, was undertaken with the intention of understanding how dynamically varying solution-phase structures relate to static solid-state crystalline structures.

Structural Analysis of Pyrazine-Bridged Molecular Square (1). Due to its small size, square **1** should be minimally flexible. Figure 3 compares the experimental solution-phase wide-angle X-ray scattering pattern with a scattering pattern calculated from previously measured single-crystal structure coordinates.[18] The two patterns generally show good agreement in interference peak positions and frequency throughout the measured range, indicating that the solution structure corresponds closely to that in the crystal. However, two important differences can be noted.

First, damping of the solution-phase scattering pattern relative to the solid-state-derived pattern is clearly evident, particularly in the q-range above 3 Å^{-1}. The differences suggest that the solution pattern is broadened by relatively low amplitude structural dispersions (atomic displacements <2 Å). Molecular dynamics simulations confirm that torsional flexibility of this magnitude exists for **1**, with the distribution of torsional angles about the improper torsion axis of Re−Re−Re−Re being less than 5°.

Second, the solution-phase scattering pattern for **1** shows features that deviate from those expected from intramolecular scattering alone. For example the experimental data show an additional peak near $q = 1.2$ Å^{-1} (Figure 3) that is absent from the intramolecular scattering calculated from the crystal structure and is distinguishable from the scattering measured for neat solvent. X-ray diffraction patterns of neat solvents are characterized by a prominent "first sharp diffraction peak" that reflects the liquid packing of solvent molecules and vary with temperature, chemical characteristics of the solvent, and solvent−solvent interactions.[38−40] The solvent diffraction peak for dimethylformamide occurs at $q = 1.38$ Å^{-1} at room temperature (see Figure S1, Supplemental Information). The presence of an additional peak near $q = 1.2$ Å^{-1} that cannot be correlated with intramolecular scattering or with scattering from a neat solvent suggests that **1** is associated with a perturbed solvation layer analogous to the larger solvent reordering that has been observed from X-ray diffraction measurements from ionic supramolecular[36] and metal ion solutions.[25,37]

(38) Badyal, Y. S.; Saboungi, M.-L.; Price, D. L.; Shastri, S. D.; Haeffner, D. R.; Soper, A. K. *J. Chem. Phys.* **2000**, *112*, 9206−9208.
(39) Morineau, D.; Alba-Simionesco, C. *J. Chem. Phys.* **1998**, *109*, 8494−8503.
(40) Vahvaselkä, K. S.; Serimaa, R.; Torkkeli, M. *J. Appl. Crystallogr.* **1995**, *28*, 189−195.

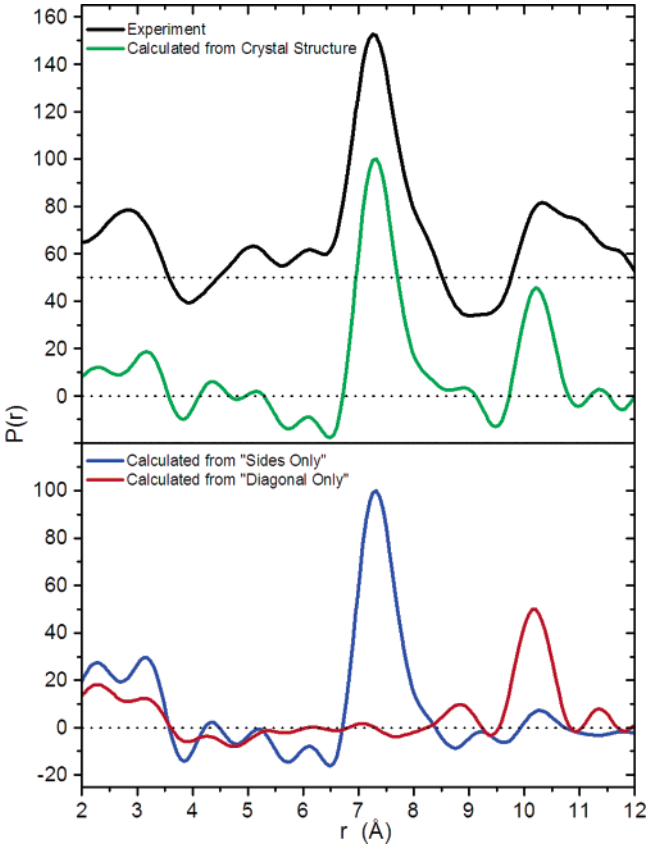

Figure 4. Experimental and crystal coordinate model determined PDF correlations for the pyrazine-bridged square. Top panel: The black line shows the experimental solution-phase PDF profile, while the green line shows the PDF profile derived from crystallographic data for the complete square. For clarity, these patterns are arbitrarily vertically offset. Bottom panel: The blue line shows the PDF calculated for an isolated "edge" pair of $Re(CO)_3Cl$ moieties at positions given by the crystal structure, but with the atoms of the pyrazine edges removed. The red line shows the PDF determined using just the isolated $Re(CO)_3Cl$ diagonal pairs from the crystal structure.

Inverse Fourier transform techniques can be used to determine the real space interactions that create the interference patterns in reciprocal space. Atomic pair distribution functions were calculated from both the solution-phase and solid-state-derived scattering patterns using the program GNOM.[21] Shown in Figure 4 (top panel) are PDF correlations for the pyrazine-bridged square. In the bottom panel are hypothetical profiles calculated from the single-crystal structure by using only fragments of the structure. The blue line trace shows the PDF calculated from isolated $Re(CO)_3Cl$ pairs separated by the pyrazine side spacer, but with the pyrazine atoms removed. This partial structure calculation shows that the PDF associated with the crystallographic $Re(CO)_3Cl$ side spacing gives rise to a prominent peak at 7.3 Å. The red line trace shows the PDF determined using just the isolated $Re(CO)_3Cl$ diagonal pairs from the crystal structure. The diagonal pairs produce a PDF peak at 10.2 Å. Both peaks appear in the experimental PDF, providing a direct measurement of the dimensions of the molecular square in solution. In addition, the experimental PDF pattern shows a broadening, particularly beyond the 10.2 Å diagonal pair distance. The origin of this broadening is not known, but one possibility is that this reflects solvent association at the corners of the square, effectively increasing the dimensions of the solute−solvent assembly.

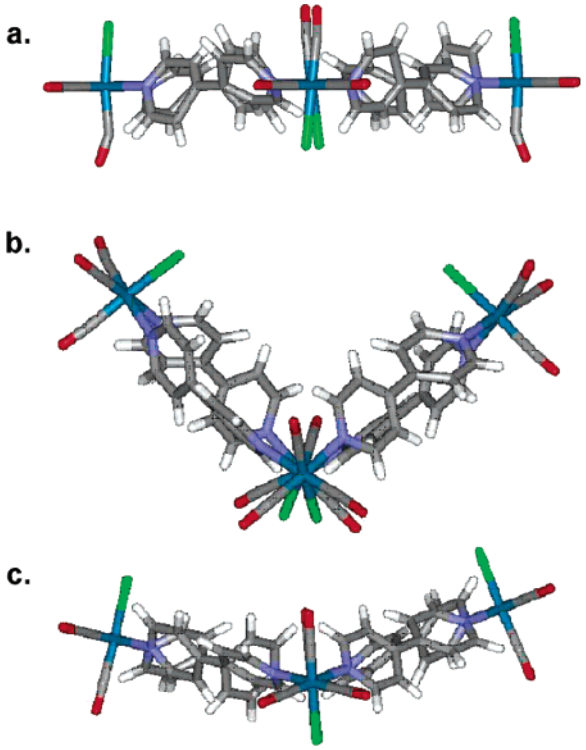

Figure 5. Crystal structures and model of bipyridine bridged molecular squares, **2**. (a) Crystal structure **2a**. Re−Re−Re−Re dihedral angle = 0. (b) Crystal structure **2b**. Re−Re−Re−Re dihedral angle = 54. (c) Lowest energy molecular model **2c**. Re−Re−Re−Re dihedral angle = 19.

Structural Analysis of Bipyridine-Bridged Molecular Square (2). Two strikingly different crystal structures exist for **2**, one with a flat geometry[18] and the other with a puckered butterfly form[17] (see Figure 5a and 5b, respectively). The flat structure has been interpreted as a cocrystal of two or more of the four possible structural isomers of **2**. In principle, the halide ligand (X) for each rhenium can be oriented either above or below the plane of the square, Figure 6. For simplicity, only one isomer is shown in Figure 5a; the single-crystal X-ray structure, however, shows equal occupancy by CO and Cl at each of the potential isomerization sites. The puckered structure, on the other hand, corresponds to a single isomer. Importantly, once formed, the isomers do not interconvert. Regardless of the interpretation of the structures, the variance implies that **2** possesses a large degree of torsional flexibility. Molecular dynamics simulations confirm that the square is indeed flexible. Results from simulated annealing yield a lowest energy conformation of intermediate geometry with respect to the crystal structures, i.e., a configuration having an improper torsion angle of about 19°, Figure 5c. One consequence of macromolecular flexibility, albeit in a materials context, could be lower porosity (and smaller permeant size cutoff) than expected for an idealized open geometry.[41]

Upon first inspection, the general features of the experimentally determined scattering pattern (i.e., frequencies and ampli-

(41) For example, molecular sieving studies with swellable (amorphous) films of porphyrinic molecular squares yielded a permeant size cut-off equaling the cavity diameter for an isolated square, while a similar study with rigid, nonswellable (amorphous) films yielded a significantly smaller size cutoff, attributed to tilting of the square's walls. See: Massari, A. M.; Gurney, R. W.; Schwartz, C. P.; Nguyen, S. T.; Hupp, J. T. *Langmuir* **2004**, *20*, 4422−4429, and Keefe, M. H.; O'Donnell, J. L.; Bailey, R. C.; Nguyen, S. T.; Hupp, J. T. *Adv. Mater.* **2003**, *15*, 1936−1939.

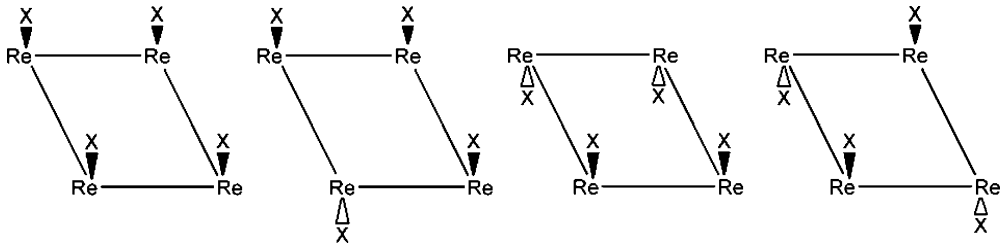

Figure 6. Four isomers can be formed for molecules having the formula $\{Re(CO)_3(X)(\mu\text{-ligand})\}_4$.

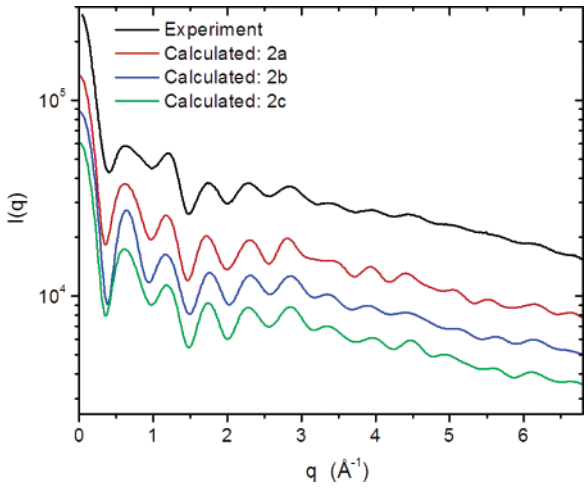

Figure 7. High angle molecular diffraction data obtained from 4,4′-bipyridine bridged molecular square in solution, simulated from crystal structures, and simulated from an energy-minimized structure. For clarity, these patterns are arbitrarily vertically offset.

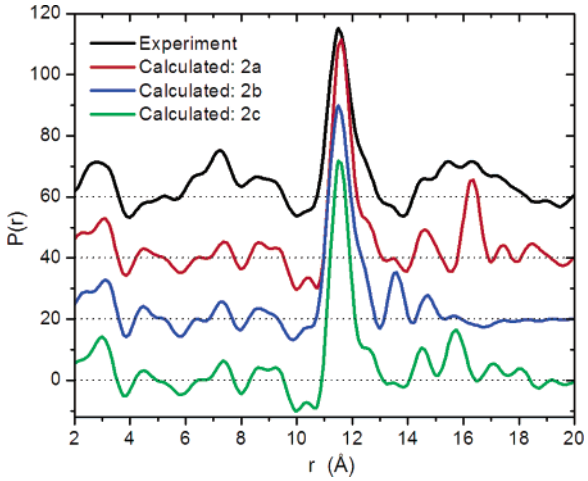

Figure 8. Pair distribution functions for bipyridine square from experiment, crystal structures, and model.

tudes) look quite similar to those generated from the two sets of crystal structure data and from molecular modeling; see Figure 7. The differences in structure are much more easily seen in real-space pair distance distribution plots, Figure 8. The differences between the four plots are most clearly evident at distances greater than the Re−Re square side distance (11.5 Å). Thus, while the experimental solution-phase PDF plot shows a broad envelope of unresolved atomic pair correlations across the 14 to 19 Å distance range, the PDF patterns calculated from the crystal and geometry-optimized model structures show well-resolved peaks that can be correlated with specific atom pair diagonal distances. Crystal structure **2b**, in which the improper

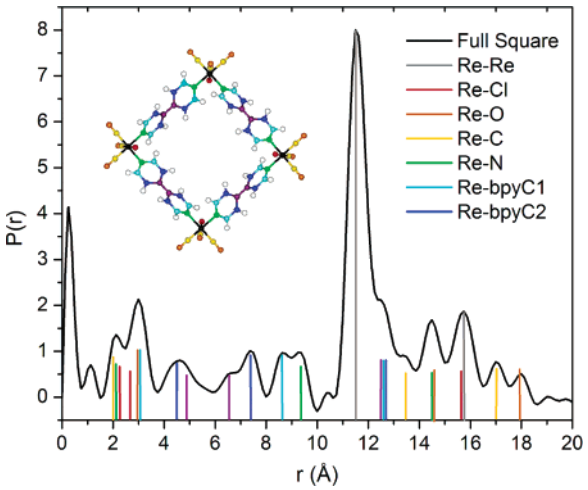

Figure 9. Line spectrum highlighting each component−Re interaction distance. The heights of the peaks represent electron density weighted contributions of each of the interacting pairs as calculated from structure **2c**.

Re−Re−Re−Re torsional angle is 54°, shows the shortest correlation peaks that are condensed to two prominent peaks at 13.6 and 14.7. The flat crystal structure **2a** shows the longest diagonal pair distances that resolve into four peaks within the 14 to 19 Å range. The diagonal pair correlation for the molecular model **2c** is intermediate between the other two models. The diagonal PDF peaks for crystal structure **2b** fall outside the experimental envelope of distances, indicating that this solid-state structure does not make a significant contribution to the ensemble of solution state structures. Diagonal PDF peaks for structures **2a** and **2c** fall within the experimental envelope. However, broadening of experimental correlation peaks in the 14−19 Å window indicates that multiple configurations are likely to contribute to the solution structure as well.

We consider the consequences of multiple conformations further below. First, however, in order to understand better what physical distances within the molecule are contributing to the pair distribution function, the molecular model was broken down into component scattering pairs. It was found that due to the high electron density on the Re atoms, the only pair correlations that contributed significantly to the overall plot are those of Re−Re or Re−A, where A is any other non-hydrogen atom in the square (C, O, N, Cl). Even the Cl−Cl interaction, the next largest scattering pair in the square after the various Re−A, was not large enough to be picked out from the overall scattering pattern. Figure 9 shows a complete Re−A (and Re−Re) structural decomposition of **2** with a vertical line corresponding to each of the peaks in the overall PDF plot. The plot was constructed using the static model (**2c**) geometry. Peaks in the experiment can be aligned with specific Re−A (or Re−Re)

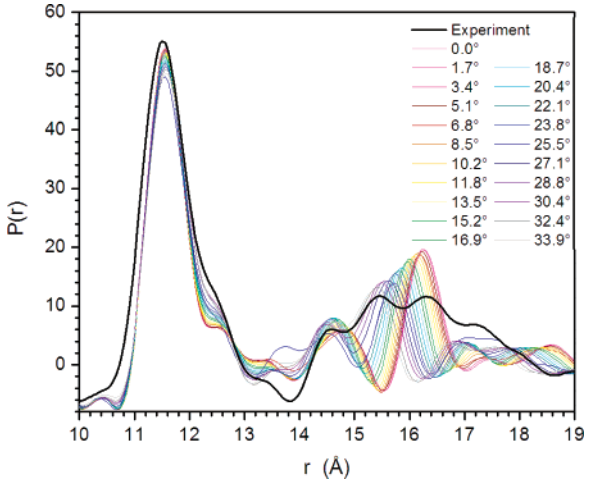

Figure 10. Pair correlations for molecular models with torsional angles ranging from 0° to 34°.

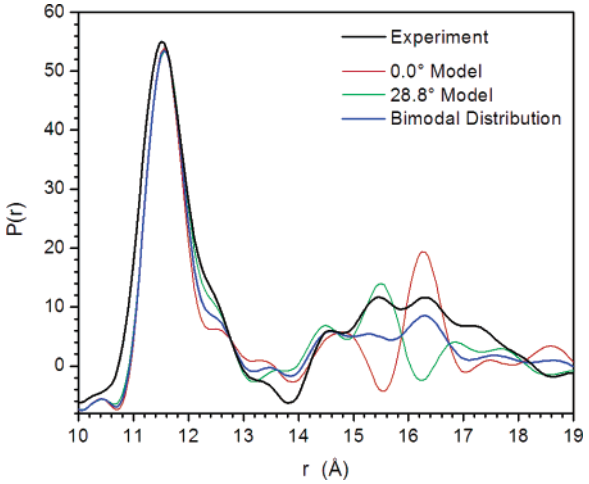

Figure 11. Pair correlations of molecular models representing a bimodal distribution of conformers in solution.

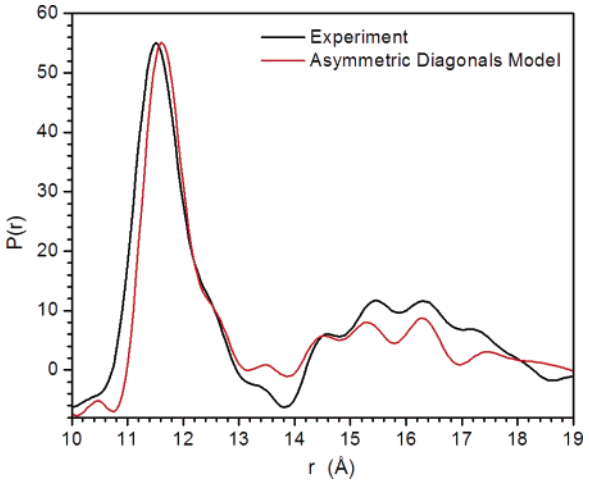

Figure 12. Pair correlation for a model with asymmetric diagonals.

distances in the model. Notably, the atomic correlations that contribute most significantly to the peaks found at longest distances are those due to the Re−Re diagonals and to carbonyls interacting with remote (i.e., diagonal) Re atoms.

To gauge the effects of conformational variations, molecular dynamics simulations were run. The simulations revealed a pronounced butterfly type flexibility, with the most highly puckered conformation having a torsional angle of 36°. In order to generate a dynamic model of the molecule, Re−Re−Re−Re configurations were modeled for a number of torsion angles ranging from 0° to 34°. Analysis of rhenium-only PDF data shows that the diagonal Re−Re distance varies about 1 Å over this range of torsion angles.

To understand in more detail the effects of torsional flexibility on the pair distribution functions, ligands were added to the Re-only models and then optimized in Hyperchem without perturbing the locations of the rhenium atoms. Once the models were generated for each angle, the corresponding pair distribution functions were calculated. These are shown in Figure 10, along with the experimentally determined pair correlation (bold black line). While the range of diagonal atomic pair correlations produced by the MD ensemble are seen to fall within the experimental envelope, the population weighted average of the MD conformers produces an ensemble envelope with two resolved peaks centered at 14.6 Å and 16.1 Å that differs significantly from the broad experimental envelope where four partially resolved maxima can be discerned. Thus, the simplest treatment of conformational effects appears to account for much of the experimental PDF envelope but does not account for full broadening and appearance of multiple unresolved peaks. Below we consider three further potential contributions to the experimental plot.

One possibility is a shift of the solution ensemble toward a bimodal distribution of torsion angles, associated with fluctuations between two limiting conformers, one flat and one puckered, although not as severely puckered as observed in crystal structure **2b**. Indeed, the most frequently occurring conformations in the MD simulations are those centered at torsional angles between 0° and 4° and between 24° and 28° (see Figure S3, Supporting Information). PDF plots for conformers within these two discrete ranges were averaged to produce a single trace for a bimodal distribution in Figure 11. The resulting PDF envelope shows three partially resolved peaks that are aligned reasonably well with the experimental trace between 14.5 and 17 Å. However, there are clear variances between the bimodal model and experimental PDF patterns. For example, the model does not reproduce the region of negative electron density (compared to the average solvent electron density) between 13 and 14 Å and fails to capture additional positive intensity between 17 and 19 Å. We note that the structure of the solvent−solute interface can contribute to both of these features and discuss these further below.

A second possible mechanism for bringing experimental and model PDF patterns into closer agreement centers on the introduction of asymmetric distortions in the molecular models. We have considered the effects of reducing the pseudo-4-fold symmetry of the molecular squares to a 2-fold plane of symmetry. This renders the two Re−Re diagonals inequivalent. Asymmetric distortions of this sort are not seen in crystal structures or in geometry-optimized models, but they reproduce several features of the experimental plot. Moderate asymmetric puckering (with an overall improper torsion angle of 24°) yields inequivalent Re−Re distances of 15.5 Å and 16.3 Å (Figure S4). As shown in Figure 12, the asymmetric model yields four major peaks in the pair correlation between 14 and 17 Å rather

than the two observed for higher symmetry models. Nevertheless, the agreement is not exact in this region.

A third consideration involves contributions due to the structure at the molecule−solvent interface. Solution PDF patterns reflect the solvent contrasted electron density weighted atom−atom pair correlations. For model calculations, the electron density distribution for each atom is described by the atomic form factors contained within van der Waals derived solvent excluded volumes.[33−35] Features of negative amplitude in the calculated PDF patterns arise from regions of the molecule where the atomic electron density within the solvent excluded volume is lower than the average electron density of the solvent. This includes minima that appear in both the experimental and model-calculated PDF near 4 Å, 10 Å, and 14 Å. Positions of maxima and minima are found to be in quite good agreement for the experimental and model-calculated PDF for square **2** in the distance range below 12 Å (Figure 8), indicating that atomic pair correlations are relatively fixed along the molecular sides and that atomic solvent excluded volumes are reasonably well-parametrized in model calculations. These findings support the interpretation that variances between model and experiment are likely to arise from solvent−solute interactions and solute configurational dispersion rather than inaccuracies in calculation of the PDF themselves. One observable variance between experimental and calculated PDF patterns occurs in the 6−8 Å region where the experimental PDF shows stronger correlations than model calculations. Solvent ordering or preferential solvent association with the molecular square could yield additional atomic pair correlations that are currently absent in model calculations. Analogous sources for deviation were seen in the scattering data for square **1** and have been reported for supramolecular assemblies[36] and metal ions in solution.[25,37] These considerations indicate that solution wide-angle scattering data can be analyzed to provide insights into both supramolecular conformation and the structure of the molecule−solution interface. Understanding these effects in a solvent-explicit atomistic simulation is a focus of current efforts.

Conclusions

Wide-angle X-ray scattering was used to quantify dimensions of rhenium-based molecular squares in dilute solution environments. Multiple atomic pair correlations were identified and quantified with high resolution (1 Å). The most prominent of these, the Re−Re edge distance, agrees well with crystallographic and/or modeling data for each of the four assemblies studied, pointing to the general quantitative validity and utility of this approach for gauging heavy-atom/heavy-atom separation distances for this class of systems. The measurements additionally reveal that the smallest square examined, **1**, possesses a solution-phase structure that is similar to that in the crystalline solid state. The solution-phase structure of square **2**, on the other hand, differs from that obtained from either of two solid-state single crystal measurements. The structure appears to be best described by a bimodal distribution of conformers that are interrelated by a butterfly type motion spanning about 25° in the improper Re−Re−Re−Re torsion angle. Preliminary molecular dynamics simulations support this interpretation. Additionally, the measurements provide strong evidence for ordering of solvent molecules by the supramolecular assemblies. We are currently seeking to obtain a quantitative understanding of the solvent ordering effects and of closely related host−guest interactions. We are also seeking to extend the approach to real-time dynamics, in particular the dynamics and associated structural changes of photoinitiated supramolecular processes.

Acknowledgment. We thank the Office of Science, U.S. Department of Energy for support of our work (Grant DE-FG02-01ER15244 to Northwestern and Contract DE-AC02-06CH11357 to the Argonne National Laboratory). J.L.O. gratefully acknowledges a fellowship from the Argonne Lab-Grad Program. We are also especially appreciative of the expert help of the Sector 12 staff at the Advanced Photon Source and, in particular, that from Drs. Soenke Seifert and Nadia Leyarovska. We also thank Dr. Shih-Sheng Sun for providing samples of compounds **1** and **4**, Dr. Christopher Graves for providing samples of compound **3**, and Mr. Manohar Murthi for helpful discussions.

Supporting Information Available: Experimental Methods including synthesis, data collection, and molecular modeling. Background subtractions and data correction method for obtaining solution-phase wide-angle X-ray scattering patterns, with Figure S1 showing raw data, solvent background, and subtraction of background; Figure S2 showing data corrections; Figure S3 showing molecular dynamics histogram of conformers; and Figure S4 showing a molecular square distortions with lower symmetry.

JA0659065